COMPUTATIONAL ASTEROSEISMOLOGY

by

TRAVIS SCOTT METCALFE, B.S., M.A.

DISSERTATION

Presented to the Faculty of the Graduate School of

The University of Texas at Austin

in Partial Fulfillment

of the Requirements

for the Degree of

DOCTOR OF PHILOSOPHY

THE UNIVERSITY OF TEXAS AT AUSTIN

August 2001

Chapter 5

Reverse Approach

> "The only real voyage of discovery consists not in seeking new land-
> scapes but in having new eyes."
>
> —*Marcel Proust*

5.1 Introduction

The results of forward modeling with one adjustable point in the chemical profile
make it clear that information about the internal structure is contained in the
data, and we just need to learn how to extract it. If we want to test more compli-
cated adjustable profiles, forward modeling quickly becomes too computationally
expensive as the dimensionality of the search space increases. We need to devise
a more efficient approach to explore the myriad possibilities.

The natural frequency that dominates the determination of pulsation periods
in white dwarf models is the Brunt-Väisälä (BV) frequency, which we calculate
using the Modified Ledoux treatment described in Tassoul, Fontaine & Winget
(1990). To get a sense of how the pulsation periods depend on the BV frequency
in various regions of the model interior, we added a smooth perturbation to
the best-fit model of GD 358 from Table 4.2, moving it one shell at a time
from the center to the surface. The perturbation artificially decreased the BV
frequency across seven shells, with a maximum amplitude of 10 percent. We
monitored the effect on each of the pulsation periods as the perturbation moved

outward through the interior of the model. The results of this experiment for
the pulsation periods corresponding to those observed in GD 358 are shown in
Figure 5.1. Essentially, this experiment demonstrates that the pulsation periods
are sensitive to the conditions all the way down to the inner few percent of the
model. Since the observational uncertainties on each period are typically only
a few hundredths of a second, even small changes to the BV frequency in the
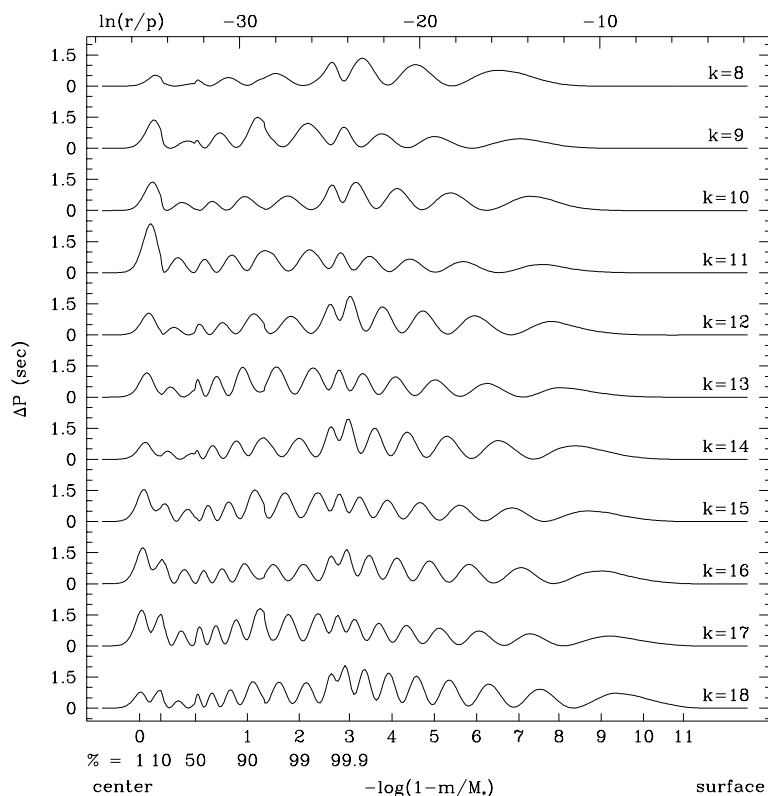model interior are significant.

Figure 5.1: For the best-fit model of GD 358 from Table 4.2 this plot shows the
change in pulsation period for $\ell = 1$ modes of various radial overtone number (k)
which result from a smooth artificial 10% decrease in the Brunt-Väisälä frequency
as a function of the natural log of the ratio of the distance from the center of
the model to the local pressure (top axis) and the fractional mass coordinate
$-\log(1 - m/M_*)$ (bottom axis). The center of the model is to the left, and
the surface is to the right. Also indicated is the mass fraction expressed as a
percentage for several values closer to the center.

5.2   Model Perturbations

The root-mean-square (r.m.s.) residuals between the observed pulsation periods in GD 358 and those calculated for the best-fit from forward modeling are still much larger than the observational noise. This suggests that either we have left something important out of our model, or we have neglected to optimize one or more of the parameters that could in principle yield a closer match to the observations. To investigate the latter possibility, we introduced *ad hoc* perturbations to the BV frequency of the best-fit model to see if the match could be improved. Initially, we concentrated on the region of the Brunt-Väisälä curve that corresponds to the internal chemical profile.

If we look at the BV frequency for models with the same mass, temperature, helium layer mass, and central oxygen mass fraction but different internal chemical profiles (see Figure 5.2) it becomes clear that the differences are localized. In general, we find that changes in the composition gradient cause shifts in the BV frequency. Moving across an interface where the gradient becomes steeper, the BV frequency shifts higher; at an interface where the gradient becomes more shallow, the BV frequency shifts lower. The greater the change in the gradient, the larger the shift in the BV frequency.

5.2.1   Proof of Concept

We began by generating a model with the same mass, temperature, helium layer mass, and internal composition as the best-fit from Table 4.2, but using a uniform internal chemical profile with constant 20:80 C/O out to the 95 percent mass point. We identified a sequence of 100 shells in this model spanning a range of fractional mass from 0.20 to 0.97 and perturbed the BV frequency to try to produce a better match to the observations. We parameterized the perturbation as a linearly varying multiplicative factor applied to the BV frequency over a range of shells, described by four parameters: (1) the innermost shell to perturb, (2) the magnitude of the perturbation at the innermost shell, (3) the number of shells in the perturbation range, and (4) the magnitude of the perturbation at the outermost shell. These 4 parameters are sufficient to describe a profile with two abrupt changes in the composition gradient.
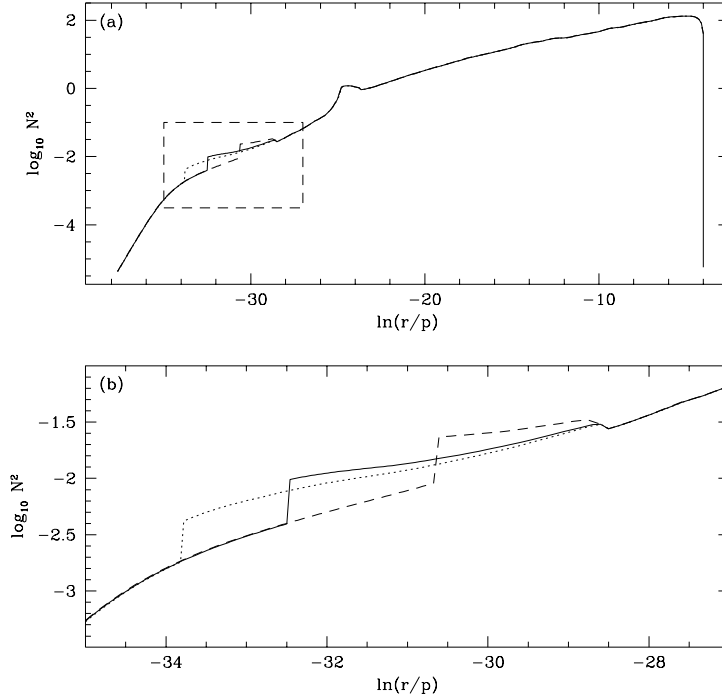
Figure 5.2: The Brunt-Väisälä frequency as a function of the radial coordinate $\ln(r/p)$ for several models with the same mass, temperature, helium layer mass, and central oxygen mass fraction but different internal chemical profiles (a) from the center of the model at left to the surface at right, and (b) only in the range of $\ln(r/p)$ indicated by the dashed box in the upper panel. The three curves correspond to a profile with q equal to 0.2 (dotted), 0.49 (solid), and 0.8 (dashed).

The innermost shell was allowed to be any of the 100 shells, and the number of shells in the perturbation range was allowed to be between 0 and 100. If the chosen range would introduce perturbations outside of the sequence of 100 shells, the outermost of these shells was the last to be perturbed. The magnitude of the perturbation was allowed to be a multiplicative factor between 1.0 and 3.0 at both the innermost and outermost perturbed shells, and was interpolated linearly in the shells between them.

By using a GA to optimize the perturbation, we can try many random possibilities and eventually find the global best-fit with far fewer model evaluations than a full grid search of the parameter-space. We demonstrated this by in-

troducing a particular perturbation to the model and determining the pulsation periods. Using the same unperturbed model, we then attempted to find the parameters of the perturbation by matching the periods using the GA. In 9 out of 10 runs (500 generations of 64 trials), the GA found a first-order solution within two grid points of the input perturbation. Thus, the GA combined with a small (625 point) grid search yields a 90 percent probability of success for an individual run. By repeating the process several times, the probability of finding the correct answer quickly exceeds 99.9 percent, even while the number of model evaluations required remains hundreds of times lower than a full grid of the parameter-space.

5.2.2   Application to GD 358

Having demonstrated that the method works on calculated model periods, we applied it to the observed pulsation periods of GD 358. We began with a model similar to the 5-parameter best-fit determined from forward modeling, but again using a uniform internal chemical profile (constant 16:84 C/O out to 0.95 m/M_*). After the GA had found the best-fit perturbation for GD 358, we reverse-engineered the corresponding chemical profile.

To accomplish this, we first looked in the unperturbed model for the fractional mass corresponding to the innermost and outermost shells in the perturbation range. We fixed the oxygen abundance to that of the unperturbed model from the center out to the fractional mass of the innermost perturbed shell. The size of the shift in the BV frequency is determined by how much the composition gradient changes at this point, so we adjusted the oxygen abundance at the fractional mass of the outermost perturbed shell until the change in the gradient produced the required shift. Finally, we fixed the oxygen abundance to that value from the outermost perturbed shell out to a fractional mass of 0.95, where it abruptly goes to zero.

After we found the C/O profile of the best-fit perturbation in this way, we fixed this reverse-engineered profile in the models and performed a new fit from forward modeling with the GA to re-optimize the mass, temperature, helium layer mass, and central oxygen mass fraction. The BV curve of the final model differs slightly, of course, from that of the original uniform composition model with the

perturbation added. But the approximate internal structure is preserved, and leads to a better match to the observed pulsation periods than we could have otherwise found.

5.3   Results

The calculated periods and period spacings ($\Delta P = P_{k+1} - P_k$) for the best-fit models from the 5-parameter forward modeling and from the reverse approach are shown in the bottom two panels of Figure 5.3 along with the data for GD 358. The best-fit models of Bradley & Winget (1994b) and Metcalfe, Nather & Winget (2000) are shown in the top two panels for comparison. The data in Figure 5.3 for the observations and our best-fit models are given in Table 5.1. Some of the improvement evident in the panels of Figure 5.3 is certainly due to the fact that we have increased the number of free parameters. To evaluate whether or not the new models represent a *significant* improvement to the fit, we use the Bayes Information Criterion (BIC), following Montgomery, Metcalfe & Winget (2001).

The fits listed in Table 4.2 used $n_p = 3$ completely free parameters, sampling several combinations of two additional parameters. This amounts to a partial

Table 5.1: Periods and Period Spacings for GD 358 and Best-fit Models

|	Observed		3-par fit		5-par fit		7-par fit	
k	P	ΔP	P	ΔP	P	ΔP	P	ΔP
08...	423.27	40.96	422.31	42.26	422.36	40.92	422.75	39.69
09...	464.23	37.36	464.57	36.77	463.28	38.01	462.43	37.46
10...	501.59	40.16	501.35	35.88	501.29	37.50	499.90	39.70
11...	541.75	35.01	537.23	39.04	538.79	36.77	539.60	36.65
12...	576.76	41.52	576.27	42.79	575.56	43.33	576.25	42.10
13...	618.28	40.07	619.06	39.79	618.89	39.85	618.36	40.25
14...	658.35	42.29	658.85	42.97	658.74	42.36	658.61	42.90
15...	700.64	33.66	701.82	32.76	701.10	34.33	701.51	33.44
16...	734.30	36.37	734.58	36.92	735.42	36.99	734.95	36.59
17...	770.67	40.03	771.50	39.30	772.41	37.34	771.54	39.60
18...	810.7	44.1	810.80	44.34	809.75	44.63	811.14	44.15
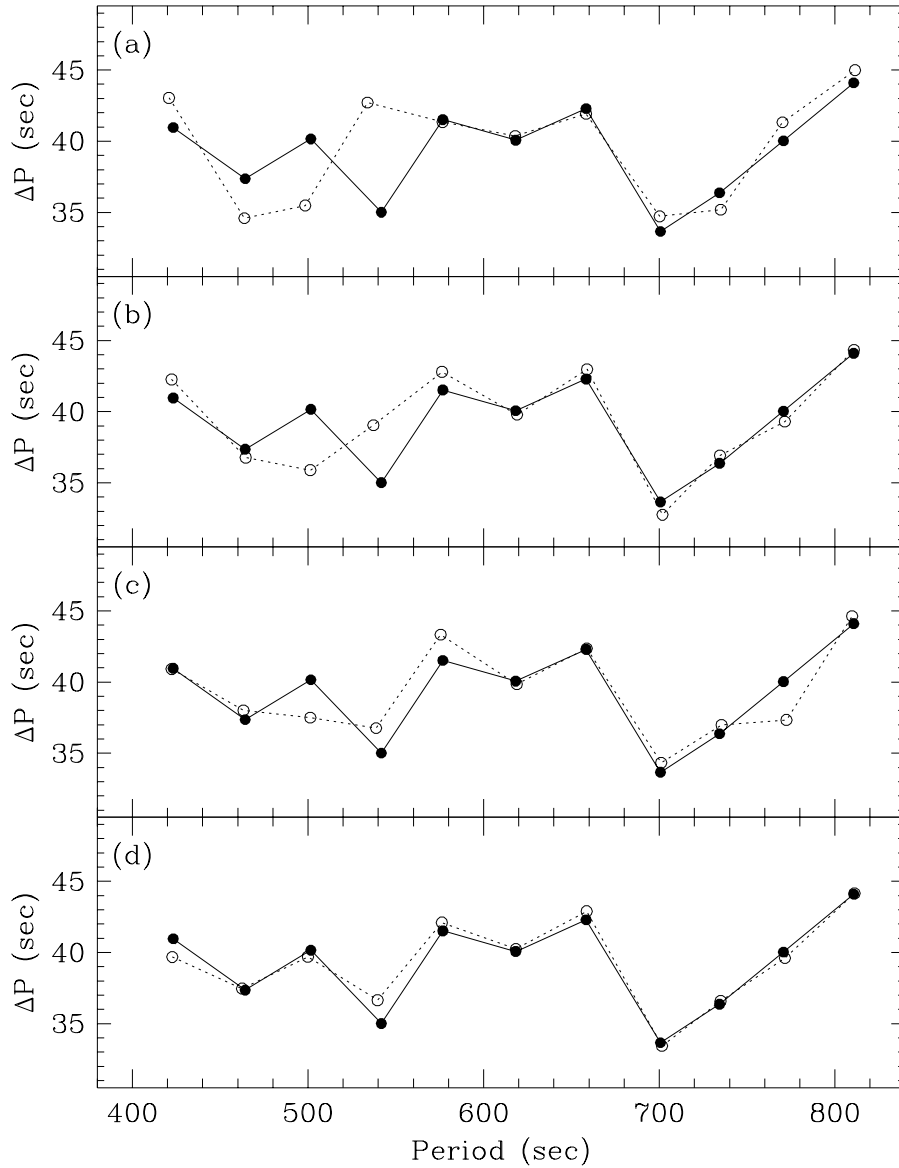
Figure 5.3: The periods and period spacings observed in GD 358 (solid points) with the theoretical best-fit models (open points) from (a) Bradley & Winget (1994b), (b) Metcalfe, Nather & Winget (2000), (c) the 5-parameter forward modeling presented in §4.6, and (d) the reverse approach. Uncertainties on the observations are smaller than the size of the points in this figure.

optimization in 5 dimensions. To make a fair comparison we use the best carbon-core model from Table 4.2, which represents the best truly 3-parameter fit. This model had r.m.s. residuals of $\sigma(P) = 2.30$ seconds for the periods and $\sigma(\Delta P) = 2.65$ seconds for the period spacings. For $N = 11$ data points, the BIC leads us to expect the residuals of a $n_p = 5$ fit to decrease to $\sigma(P) = 1.84$ and $\sigma(\Delta P) = 2.13$ just from the addition of the extra parameters. In fact, the fit from the forward modeling presented in §4.6 has $\sigma(P) = 1.28$ and $\sigma(\Delta P) = 1.42$, so we conclude that the improvement is statistically significant.

The results of the reverse approach presented in §5.2 are harder to evaluate because we are perturbing the BV frequency directly, rather than through a specific parameter. We consider each additional point in the internal chemical profile where the composition gradient changes to be a free parameter. Under this definition, the perturbed models are equivalent to a 7-parameter fit since there are three such points in the profiles, compared to only one for the 5-parameter case. If we again use the BIC, we expect the residuals to decrease from their $n_p = 5$ values to $\sigma(P) = 1.03$ and $\sigma(\Delta P) = 1.14$ seconds. After re-optimizing the other four parameters using the profile inferred from the reverse approach, the residuals actually decreased to $\sigma(P) = 1.11$ and $\sigma(\Delta P) = 0.71$ seconds. The decrease in the period residuals is not significant, but the period spacings are improved considerably. This is evident in the bottom panel of Figure 5.3.

5.4   Chemical Profiles

The internal chemical profiles corresponding to the best-fit models from the 5-parameter forward modeling and from the reverse approach are shown in Figure 5.4 with the theoretical profile for a 0.61 $M_\odot$ model from Salaris et al. (1997), scaled to a central oxygen mass fraction of 0.80. The profile from the best-fit forward modeling matches the location and slope of the initial shallow decrease in the theoretical profile. The reverse approach also finds significant structure in this region of the model, and is qualitatively similar to the Salaris et al. (1997) profile to the extent that our parameterization allows. It is encouraging that both approaches agree with each other and bear some resemblance to the models.
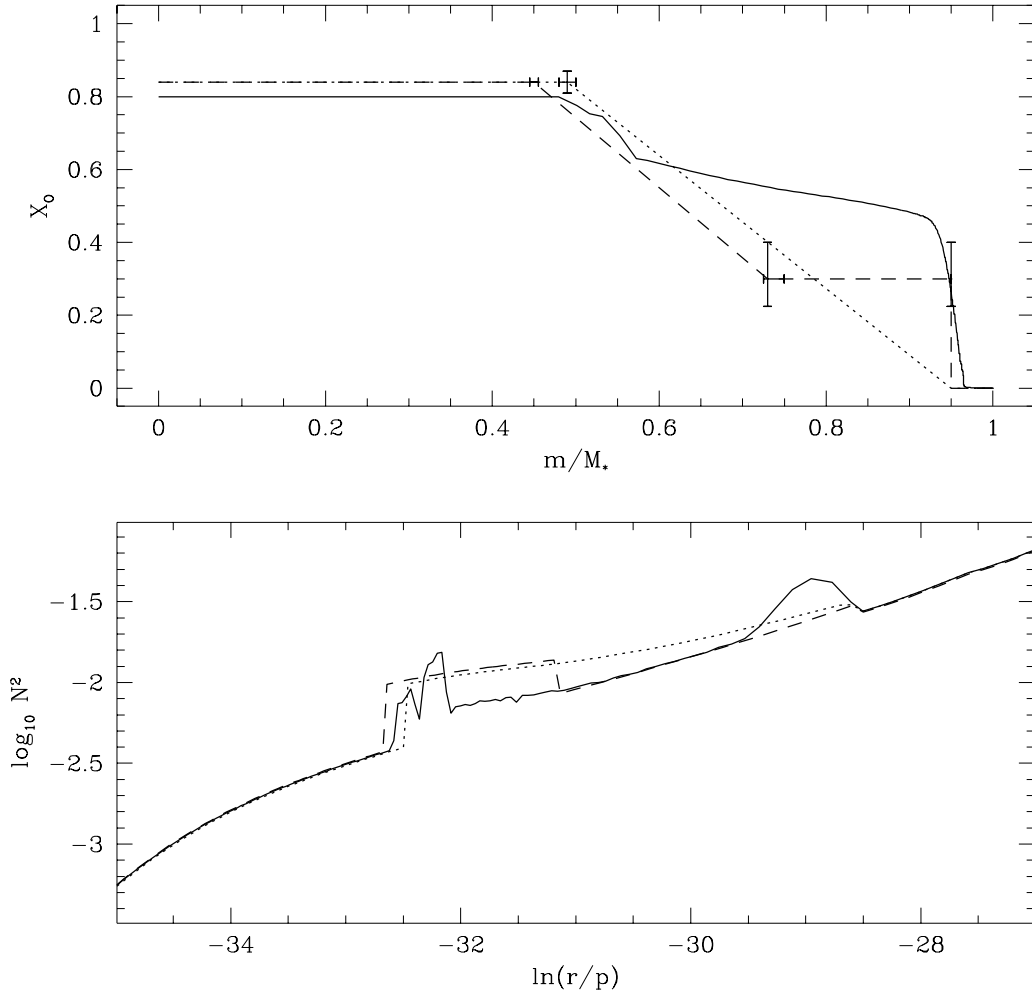
Figure 5.4: The internal oxygen profiles (top) and the corresponding region of the Brunt-Väisälä curves (bottom) for the best-fit forward model from §4.6 (dotted), the result of the best-fit reverse approach from §5.2 (dashed), and the scaled theoretical calculations of Salaris et al. (1997) for comparison (solid).